Chapter 2
Description and Classification of Prominences

Oddbjørn Engvold

Abstract Solar prominences are bright cloud-like structures when observed beyond the solar limb and they appear as dark filamentary objects which are termed filaments when seen against the solar disk. The aims of prominence classifications were from the start to establish references and frameworks for understanding the physical conditions for their formation and development through interplay with the solar magnetic environment. The multi-thermal nature of solar prominences became fully apparent once observations from space in UV, VUV, EUV and X-rays could be made. The cool prominence plasma is thermally shielded from the much hotter corona and supported in the field of gravity by small- and large-scale magnetic fields of the filament channels. High cadence, subarcsecond observing facilities on ground and in space have firmly proven the highly dynamic nature of solar prominences down to the smallest observed structural sizes of 100 km. The origin of the ubiquitous oscillations and flowing of the plasma over a variety of spatial and temporal scales, whether the cool dense plasma originates from below via levitation, injections by reconnection or results from condensation processes, are central issues in prominence research today. The unveiling of instabilities leading to prominences eruptions and Coronal Mass Ejections is another important challenge. The objective of this chapter is to review the main characteristics of various types of prominences and their associated magnetic environments, which will all be addressed in details in the following chapters of this book.

2.1 Introduction

Early solar astronomers could observe prominences only at the rare occasions of total solar eclipses until J. Janssen and Sir Norman Lockyer independently discovered with the use of spectroscopes that the luminous prominences radiated in a very few spectral lines. Their reddish color was due to the dominant Hα line of hydrogen at λ6562.8 Å. Hale (1903) and Deslandres (1910) realized both that dark

O. Engvold (✉)
University of Oslo, Blindern, Institute of Theoretical Astrophysics, Oslo, Norway
e-mail: oengvold@astro.uio.no

filaments seen in absorption on the disk were prominences seen against a brighter background. In this book the term filament is generally synonymous to prominence seen on the disk.

The EUV, far-EUV and X-ray spectral regions contain numerous emission lines formed at temperatures ranging from the photospheric to the coronal ones. Vial (2014) provides an overview of various space instruments used for prominence observations, from the early OSO satellites to the recent SDO/AIA. As an example, the main UV and EUV lines recorded with instruments on-board SOHO cover a range in ionization stages from Si II $\lambda1259$ Å and C II $\lambda1037$ Å, formed at T = 13–25×10^3 K, to O IV $\lambda554$ Å and O VI $\lambda1037$ Å representing, respectively, 2×10^5 K and 4×10^5 K (Labrosse et al. 2010). The dominant bright Hα, Ca II H and K lines, the He I at $\lambda5787$ Å and the two Na I lines at $\lambda5892$ and $\lambda5896$ Å are all emitted from the cool core prominence plasma at electron temperatures from 7.5×10^3 to 10^4 K (Poland and Tandberg-Hanssen 1983; Hirayama 1985; Tandberg-Hanssen 1995). The fact that the cool prominence structures may also be recognized in lines emitted from higher temperature plasma demonstrates that all prominences are covered by a fairly thin temperature layer which is commonly referred to as the *Prominence Corona Transition Region* (*PCTR*) (Vial 1990).

The thermodynamic parameters of the prominence plasma are derived from observed line intensities and polarization, often in combination with radiative transfer calculation and modeling (see Labrosse et al. 2010). The commonly cited cool plasma densities are 10^{10}–10^{11} cm^{-3} and gas pressure 0.1–1 dyn cm^{-2} (Hirayama 1985; Parenti and Vial 2007; Labrosse et al. 2010; Parenti 2014a). This implies that the cool prominence material is roughly 100-fold cooler than the corona gas and about 100-fold more dense. The corresponding parameters of the high temperature regions are derived from multi-wavelength observations of UV and EUV line emission by taking into account the volumes already occupied by lower temperature plasma (Anzer et al. 2007; Heinzel et al. 2008).

The first direct measurements of magnetic fields of solar prominences which were based on the Zeeman Effect are summarized in Tandberg-Hanssen (1974). Later measurements using the Hanlé effect were pioneered by the French group at Pic-du-Midi and Meudon Observatory (Leroy 1981; Bommier et al. 1994). The generally accepted typical magnetic field strength in the cool plasma is 3–30 G (Leroy 1989) implies that the ratio of the plasma pressure (p = 2nkT) cited above to the magnetic pressure ($p_{mag} = B^2/2 \mu_0$), usually referred to as *plasma-β*, then becomes 0.01–1. This implies that the magnetic fields represent the dominant force in the prominence plasma and thereby largely control their structure and dynamics. A fundamental condition for formation and development of solar prominences is clearly the local magnetic field topology rooted in the photosphere below. It is firmly established that filaments are located above the border between negative and positive magnetic fields on the Sun's surface (Martin 1998a). Comprehensive discussions of magnetic fields of solar prominences are given by Mackay et al. (2010) and López Ariste (2014).

Advancement in spatial resolution in observations from ground- and space-based telescopes provides a timely reminder that on a small-scale, and over a large range of temperatures, prominences are highly dynamic and rapidly changing in contrast to their apparent stability on the more global scale, where quiescent prominences appear relatively stable with lifetimes ranging from days up to approximately a month. Longer reported lifetimes have not been verified due to the absence of observations from the back side of the Sun and the tendency for prominences to repeatedly develop at nearly the same sites. Active prominences occurring in the vicinity of active regions are more dynamic and usually more short-lived. Active intervals or activations also occur in quiescent prominences but less frequently. The majority of prominences eventually undergo instabilities that lead to eruption and disappearance (*disparitions brusques*), most often associated with *Coronal Mass Ejections* (*CMEs*). A few prominences end their life simply by the draining of all their mass back to the chromosphere. The formation and development of solar prominences, including their fascinating variations of shape and dynamics, will be summarized in the following sections of this chapter, while the full and detailed discussions are handled in the following chapters of this book.

2.2 Classifications

A number of schemes of solar prominence classification have been proposed and are still in general use. Classifications are based on combinations of their morphology, dynamic properties and relative locations. It was early realized that prominences located close to active regions were changing quite rapidly compared with more slowly changing ones that appear in regions well removed from active regions, and at higher solar latitudes. The Italian astronomer Secchi and contemporary scientists like Respighi and Fearnley made a number of prominence drawings using wide slit spectroscopes (cf. Vial 2014). They were all struck by the variety in shapes and activity. Secchi concluded that prominences fell into two categories, one for short-lived prominences which he called *eruptives* and long-lived ones which were denoted *quiescents*.

George E. Hale's realization of the spectrohelioscope (Hale 1929) permitted more systematic observations and analysis of shapes and motions of prominences at the limb and on the disk. His instrument provided also radial velocities of the observed features. Regular spectrohelioscopic observations were subsequently initiated both at Greenwich and at Mt Wilson Observatory. Newton (1935) concluded from his studies that solar filaments and prominences were of two types; (1) those that are not associated with sunspot, and (2) those that are associated with sunspots and active regions. His measurements of radial velocities up to 100 km s^{-1} and higher were clearly associated with erupting cases. Edwin Pettit at Mt Wilson Observatory suggested a much more detailed classification scheme consisting of six main classes and several sub-classes. Pettit's classification (Pettit 1932) is illustrated below. All prominences were first divided into those connected with spots and
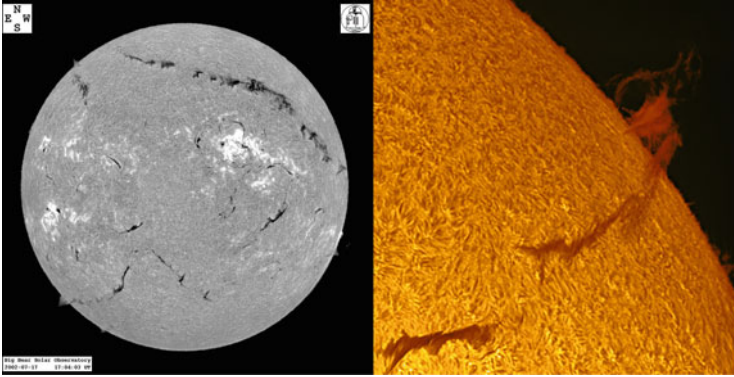
Fig. 2.1 *Left*: The full disk image observed in Balmer Hα 2002 July 17 shows a variety of filaments some located in active regions and others at high solar latitudes and away from active regions (Credit: BBSO). The *right* image (also Hα) illustrates the change from the appearance of absorbing to emitting as a filament observed on November 25, 2011 crosses the solar limb (Credit: Tom Wolfe)

those that were not. Figure 2.2 is a self-explaining comprehensive illustration of the categories and sub-categories of Pettit's classification system.

Further progress in instrumentation and photographic techniques, like Bernard Lyot's coronagraph and monochromatic filter based on birefringence of quartz and the selective transmission of polaroids (see Vial 2014), enabled Donald H. Menzel to establish routine observations of the chromosphere and prominences at the High Altitude Observatory in Colorado. A notable collection of systematic observations of prominences which also included motion pictures, led Menzel and Evans (1953) to suggest a classification scheme, which differed somewhat from Pettit's scheme. They assigned the letter *A* to prominences in which matter flows downwards from above and the letter *B* to prominences with matter flowing into the corona from below. The letter *S* was assigned to prominences connected with sunspots and *N* to the others (non-spot). There were subcategories to each of the four types as shown in the following resulting scheme:

A. Prominences originating from above in coronal space

   S. Spot prominences:

   l. Loops
   f. Funnels

   N. Non-spot prominences:

   a. Coronal rain
   b. Tree trunks
   c. Trees
   d. Hedgerows
   e. Suspended clouds
   m. Mounds

B. Prominences originating from below in the chromosphere

    S. Spot prominences

        s. Surges
        p. Puffs

    N. Non-spot prominences

        s. Spicules

In a subsequent classification scheme proposed by de Jager (1959) prominences were classified as either (I) *Quiescent* or (II) *Moving Prominences*. The quiescent prominences were grouped further into *Normal* (low to medium latitudes) and *Polar* (high latitudes). The class of *Moving Prominences* included *Active*, *Eruptive* and *Spot* (*associated*) *Prominences* plus *Surges* and *Spicules* (Fig. 2.2)

Zirin's (1966, 1988) classification of class 2 *Long-lived*, *Quiescent Prominences* was identical to de Jager's Class I, while he grouped *Loops*, *Coronal Rain*, *Surges* and *Sprays* under his Class 1 *Flare-associated*, *Short-lived Prominences*.

Any prominent solar feature seen above the rim of the Sun was historically associated with the term prominence. Increased awareness of related phenomena led to a rich "zoo" of solar features that were subsequently classified under a prominence umbrella. This included features like flare loops, surges, coronal loops or arches, various types of mass ejections, large spicules, coronal rain and coronal cloud prominences. *Surges* and *Loops*, which occur in conjunction with flare activity, are now recognized as active region jet phenomena and post flare loops, respectively, and regarded quite different from solar prominences. Furthermore, spicules constitute rather the main structure of the chromosphere. In the following chapters *Coronal Rain* and *Coronal Cloud Prominences* remain as a significantly different types of prominence.

It is quite common today to divide prominences into *Quiescent*, *Intermediate* (combined) and *Active Region Prominences*, which also will be the adopted classification in the following subsections. This simple classification evolved from the early active and quiescent designations and has remained practical with the recognition of intermediates which fill-in a broad continuum of filaments ranging from low and narrow ones in the active regions to high and wide quiescent ones. All three groupings have varied lengths from very short to extremely long (Fig. 2.1).

Although many former classifications have mostly historical interest (cf. Tandberg-Hanssen 1995) they have all served to identify and understand the physical conditions for their formation and development over a large range of spatial and temporal scales. Only coronal cloud prominences and coronal rain are sufficiently different to be under a separate heading as discussed in Sect. 2.5.

In addition to spectacular differences in morphology and dynamics, solar prominences also show notable variations in spectroscopic characteristics.

The use of spectral classifications was initiated by Martin Waldmeier (cf. Waldmeier 1970) who compared observed intensities of Mg I lines (λ5184, λ5172 and λ5167 Å) and the Fe II line λ5186 Å and showed that these line ratios were
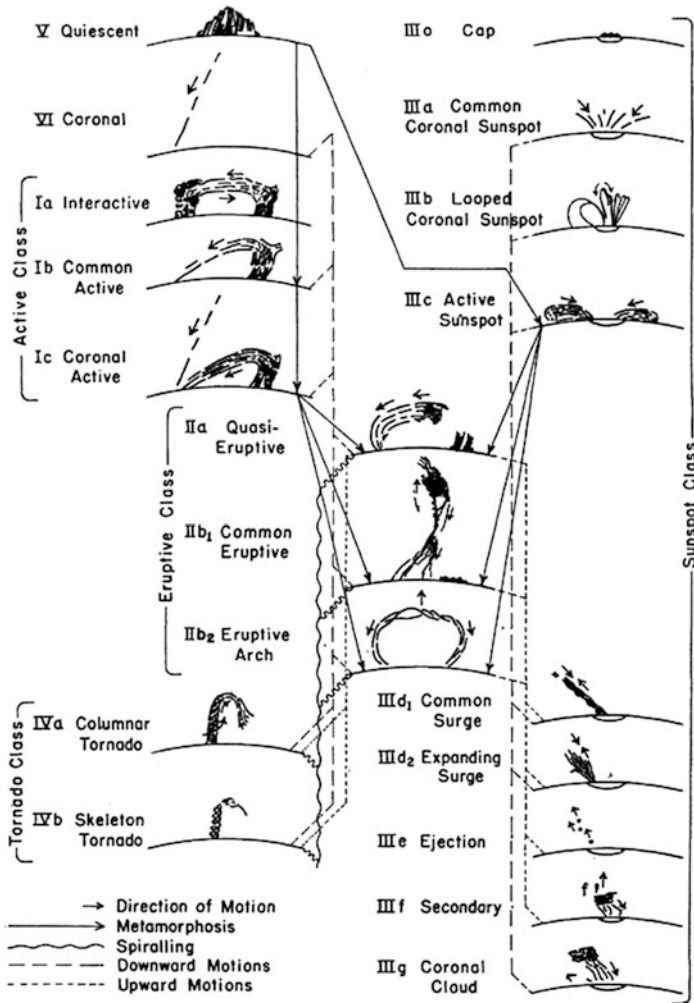
Fig. 2.2 Drawings of various types of solar prominences made from photographs. (*Credit*: Petit, 1932)

not the same in solar prominences and flares. A more detailed classification scheme was introduced by Zirin and Tandberg-Hanssen (1960) where they could distinguish quiescent prominences from active prominences and flares. Using a well-known variation with height in the chromosphere of relative intensity of neutral and ionized lines they could separate prominences into two major categories, i.e. quiescent prominences and active prominences (and flares). Their study showed that I (He II λ4686 Å) $<<$ I (He I λ4713 Å) both in the low chromosphere and in quiescent prominences, whereas these two lines are equally bright in the high chromosphere and in active prominences.

Fig. 2.3 Examples of various types of solar prominences. *Left image*: "hedgerow prominence". Middle image: "suspended cloud", which is also the same class of prominence that Pettit called coronal cloud (III g in Fig. 2.1). *Right image*: "tree prominence" (*Credit*: Richard B. Dunn)
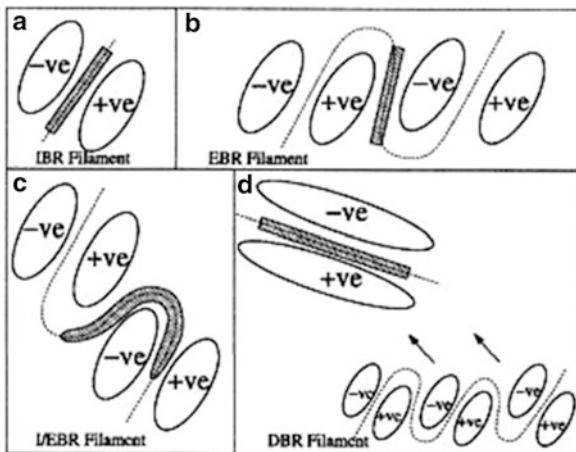

Fig. 2.4 Classification scheme for solar filaments developed by Tang (1987) and Mackay et al. (2008). (**a**) Filaments that form above the internal PIL (*Polarity Inversion Line*) of single bipoles are classified as IBR. (**b**) Those forming on the external PIL between bipoles or between bipoles and unipolar regions of flux are classified as EBR. (**c**) Filaments that lie both above the internal PIL within a bipole and the external PIL outside the bipoles are classified I/EBR. (**d**) Finally, those filaments that form in diffuse bipolar distributions resulting from flux emergence and the diffuse region can no longer be associated with any single bipole emergence are classified as DBR (*Credit*: Mackay et al. 2008)

Today's studies and analysis of the spectral emissions of solar prominences are subject to complex non-LTE radiative transfer modeling which will be covered in details in this book (Heinzel 2014; Labrosse 2014).

A new and different classification system was proposed initially by Tang (1987) and developed further by Mackay et al. (2008), with the aim to understand better where filaments form relative to the magnetic configuration in the photosphere below. The proposed four categories which are presented in Fig. 2.4 and valid for large, stable filaments, are discussed in detail by Mackay (2014).

2.3 Environments of Active Region, Intermediate and Quiescent Prominences

2.3.1 Filament Channels

Filament channels provide the magnetic environment in the low corona where filaments may form and be supported against gravity and thermally shielded from the surrounding hot corona. Channels follow along the division between opposite polarities in the line-of-sight magnetic fields measured in the photosphere, which has variously been referred to as the neutral line, *Polarity Inversion Line* (PIL) and *Polarity Reversal Boundary* (*PRB*). Filament channels tend to be long-lived and may spawn many successive filaments. After eruption of a filament on the quiet Sun, a channel may be nearly void of mass for one or more days whereas in active regions, successive filaments may form during or within a few hours after the eruption of a filament. The emergence and distribution of magnetic polarities determines where channels form (Gaizauskas 1998).

In the chromosphere filament channels are associated with fibril structures (called spicules when viewed at the solar limb) aligned along the polarity reversal boundaries (Smith 1968; Foukal 1971). Foukal also noticed that fibrils which are rooted in *plagettes* with observable magnetic polarity, stream in antiparallel directions on opposite sides of a polarity inversion (Fig. 2.5). The orientation of the fibrils implies that the magnetic field of the filament channel is predominantly horizontal and pointing in the same direction on the two sides a of the channel, as illustrated in the lower left panel of Fig. 2.5. One finds that also small coronal loops within the channels are oriented parallel with the polarity inversion boundary which implies that channel fields extend into the low corona (Wood and Martens 2003) and thereby that the most of filament axis is embedded in this horizontal field.

Similar systematic orientations of coronal cells are noticed in 1.2 MK data in the Fe XII λ193 Å line observed with the SDO/AIA instrument (Sheeley et al. 2013) (Fig. 2.5). These coronal cells have the approximate diameter of photospheric *supergranules* ∼30,000 km (Simon and Leighton 1964) but are centered over network fields at the vertices of *supergranules* rather directly over supergranules.

Martin et al. (1992) introduced the concept of chirality of filament channels. The channels were classified as either dextral or *sinistral* depending on the axial field direction observed from the positive polarity side of the channel as illustrated in the right panel of Fig. 2.6. The two columns in the left panel of Fig. 2.6 illustrate the one-to-one chirality relationships for fibril pattern (upper frames), filament spines and barbs (middle frames) and the overlying coronal loops (bottom frames).

A next major discovery was reported by Martin et al. (1994) who found a strong tendency of hemispheric dependence in location of the two chiral systems in the sense that a majority of dextral channels were observed in the northern hemisphere while the southern hemisphere harbored mainly sinistral channels. This systematic difference in the orientation of the magnetic fields of filament channels in the two hemispheres holds fundamental information on the channel formation and on the
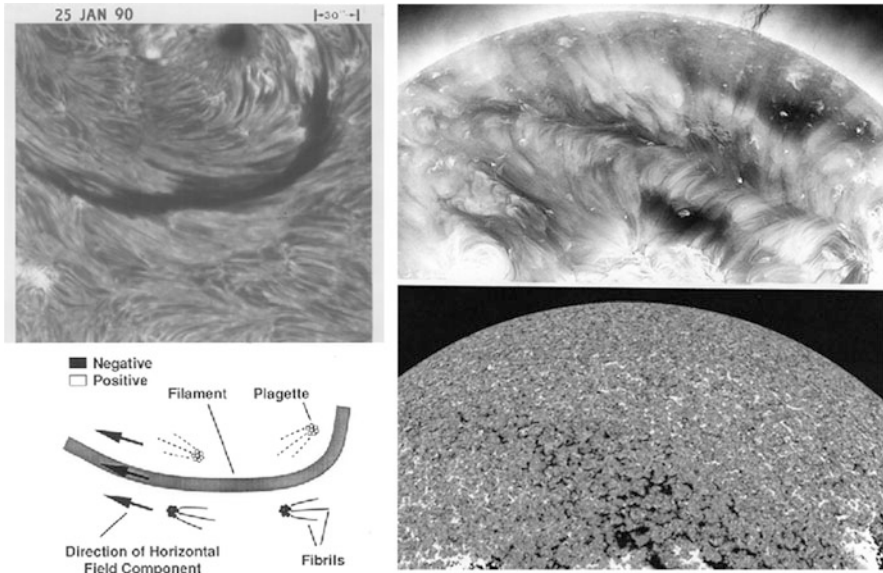
Fig. 2.5 *Left*: Illustration of opposite orientation of fibrils on the two sides of an AR Hα filament (*Credit*: Martin et al. 1992). *Right*: SDO images of a northern-hemisphere filament channel on April 23, 2012, showing cellular plumes leaning in opposite directions on the two sides a of the channel (*Credit*: Sheeley et al. 2013)

origin of solar filaments (Martin 1998a). These issues are discussed in detail by Martin (2014) and Mackay (2014).

In addition to the coronal arcades above filament channels are coronal fields seen in white-light that extend more or less radially outwards and form so-called *helmet streamers* which necessarily consist of oppositely directed magnetic fields. The magnetic arcades reach from 50,000 to 70,000 km into the solar corona while streamers extend to a solar radius or more as seen in images taken during solar eclipses.

2.3.2   Coronal Cavities

Early eclipse and coronagraphic observations showed that the filament channels contained regions of notably reduced emission between prominences and their surrounding coronal loop systems, which were subsequently referred to as coronal cavities. Some authors chose to call them prominence cavities. The total eclipse picture in Fig. 2.7 shows a bright coronal helmet streamer extending from the northeast solar limb and low-density cavity at the helmet base.

The global structure of coronal cavities is evidently shaped like tunnels, which implies that in order to measure their true brightness they must be oriented more
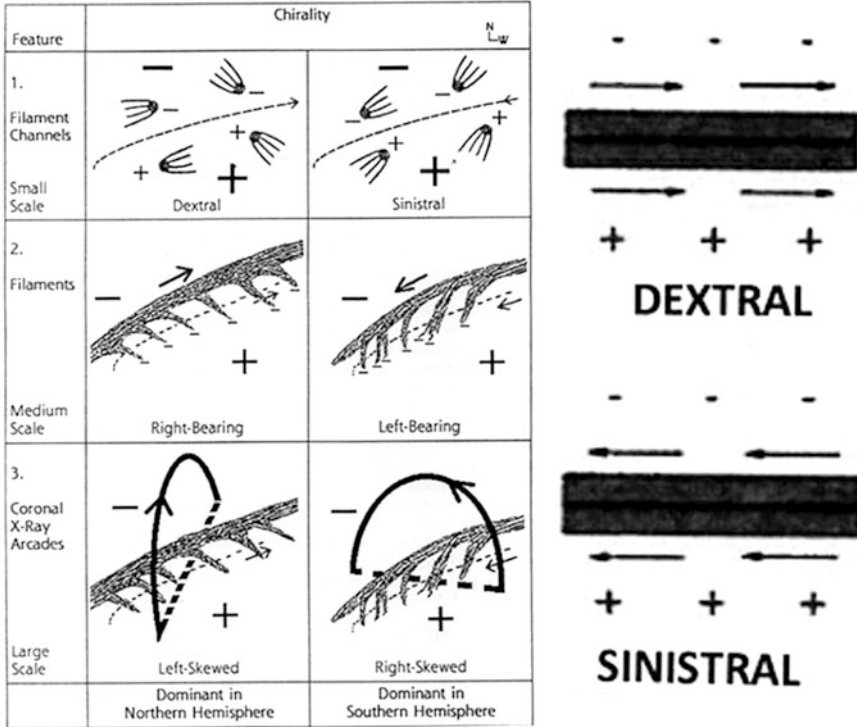
Fig. 2.6 The *left panel* shows schematic representations of the general magnetic fields of filament channels (*Credit*: Martin 1998b). The direction of the magnetic field in relation to the chirality of a dextral and a sinistral filament channel is emphasized in the *right panel* (*Credit*: Mackay et al. 2010)

or less along the line-of-sight. Therefore, largely East–west oriented high latitude channels provide most favorable conditions for brightness measurements. Emission of EUV lines formed at coronal temperatures proves that the cavities are not truly empty. Dudik et al. (2012) observed notable emission in the Fe XII λ193 Å line channel of SDO/AIA in a coronal cavity which indicates gas temperatures around 1.6 MK. Gibson (2014) shows evidence for a more multithermal situation. The reduced brightness of the cavities agrees with a plasma density that is about 30 % less than in the surrounding coronal regions (Fuller et al. 2008).

Spectral observations from the EIS instrument show the presence of large-scale flows with line-of-sight velocities $\sim$8 km s^{-1} in coronal cavities (Schmit et al. 2009). In addition, a noticeable swirling behavior of the flows is consistent with the view that cavities are filled and controlled by helically shaped magnetic flux ropes (Okamoto et al. 2010; Habbal et al. 2010; Liu et al. 2012a; Kucera et al. 2012). Three-dimensional models of coronal prominence cavity morphology are developed and discussed by Gibson et al. (2010, 2014).

Fig. 2.7 *White*-light total eclipse of 1988 March 18 showing a well-formed, bright coronal helmet streamer extending from the northeast limb, with a localized, low-density cavity at the helmet base. Within that cavity, a spatially unresolved, quiescent prominence appears as a bright blot (*Credit*: HAO/UCAR)

Recent studies by Berger et al. (2012) indicate that cavities may play a signification role in prominence formation and development. They show a pre-existing prominence disappearing slowly as a bright emission cloud forms in the regions immediately above. A subsequent prominence reformation follows a steady loss of mass by downward streaming from the cloud.

2.4   Structure and Dynamics of Active Region, Intermediate and Quiescent Solar Prominences

Typical solar prominences and filaments are composed of a *spine*, *barbs* and two extreme *ends*. The spine defines the upper main body that is oriented largely in the channel direction. The *barbs* diverge from the spines, much like exit roads of a highway, and bend down into the chromosphere and photosphere below. The ends of filaments also bend down towards the photosphere similar to regular barbs. Spines and barbs are common to both quiescent and active region prominences but the spines are much higher for quiescent prominences and the barbs are therefore also higher and can extend outward further from the spine. Barbs are not a ubiquitous feature of prominences as there are smaller short-lived active region features with no barbs while long-lasting quiescent prominences have very large barbs (Martin et al. 2008).
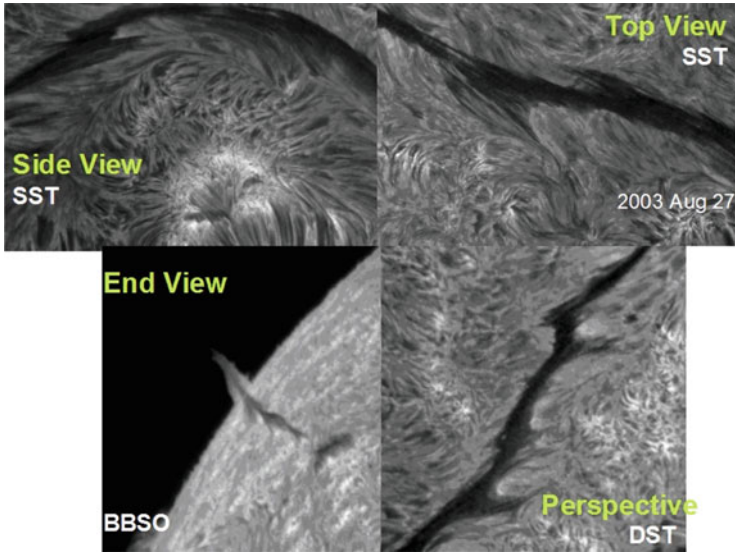
Fig. 2.8 Hα filtergrams of major sections of four intermediate filaments with a continuous spine and barbs viewed from various perspectives based on observations from the Swedish Solar Telescope (SST), the Big Bear Solar Observatory (BBSO) and the Dunn Solar Tower (DST). (*Credit*: Lin et al. 2008)

High-resolution Hα images demonstrate that spines and barbs are both composed of thin threads which constitute the fundamental structures of all solar filaments (Lin et al. 2008). Figure 2.8 contains examples of four similar prominences, intermediate between active region and quiescent filaments seen from four perspectives to provide a 3-D impression of the relative orientation of barbs to their associated spine. The upper left panel shows the side view of an active region filament. The upper right panel illustrates the top view of an intermediate filament with two independent barbs on either side of the spine. Many threads are stacked along the spine and the two barbs. The lower left panel shows an end view of a filament crossing the east limb. Here one clearly sees several barbs extending from both sides of the spine into the chromosphere. This view reveals the narrowness of the spine and shows it in absorption above the limb because it is optically thick due to many threads in the line-of-sight. In the lower right panel, a quiescent filament with several barbs is viewed partly from the side and partly from above.

Several studies have shown a notable correspondence between filament barbs and enhanced concentrations of magnetic flux located at *superganulation* cell boundaries in the photosphere below (Plocieniak and Rompolt 1973; Martin and Echols 1994; Lin et al. 2005b). The study of Martin and Echols (1994) suggested that the barbs tend to be rooted in or next to minority polarity magnetic fields on either side of the PIL.

Pevtsov and Neidig (2005) found that fragmented filaments represent the early evolution of quiescent filament development in Hα. These filaments began

their formation with a few individual "clumps" which later grow and develop interconnecting *spines* which thereby form a continuous filament body. One may assume that these "clumps" represent the start of barb formation. The magnetic structure is evidently already developed; the higher prominence body is often rather faint in Hα at the early stage in formation. Several studies have shown that the higher regions of quiescent prominences are more pronounced in the hotter He II 304 Å line compared to Hα in absorption as well as in emission (Wang et al. 1998; Lin 2000; Xu et al. 2010). This difference is most probably due to an increase with height in ionization of Hydrogen. The highly resolved Hα image in Fig. 2.11 demonstrates also that the barb consists of a number of thin threads. One notes that threads connecting with the two neighboring threads within barbs appear to be rooted in separate but closely spaced locations in the chromosphere. At the assumed bottom part of this barb the volume density of the threads becomes so high that the individual threads cannot be resolved.

2.4.1 Active Region Prominences

Active region (AR) prominences are located adjacent to sunspots. The characteristics of AR prominences are their relatively thin and straight spines. Their barbs are in general very few and less pronounced. AR prominences are relatively short-lived and subject to eruptions or major "activation" events resulting in lifetimes from several minutes to a few hours (Berger 2013).

Being closely associated with sunspot groups AR prominences correlate well in numbers and activity with the solar cycle.

Chae et al. (2001) could follow the formation of an AR filament resulting from reorientations of the local magnetic configuration in the photosphere below due to converging and shearing flows. The typical smooth, blade-like structured AR filament is displayed in the right image of Fig. 2.9, and the left image shows an AR prominence with the typically horizontal thread-structures in the spine.
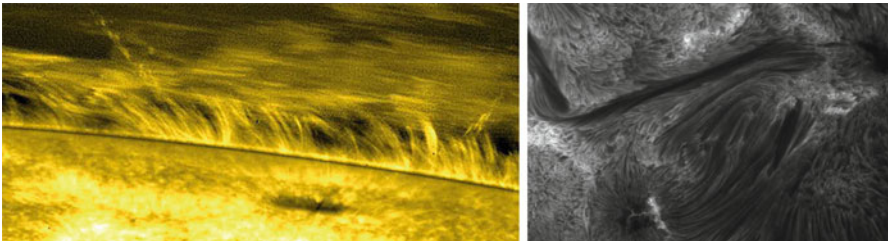

Fig. 2.9 *Right*: A slender AR filament seen in Hα obtained at the SST on 22 August 2003 is seen to have barbs extending a short distance to each side of the spine seen from above (*Credit*: The Swedish 1-m Solar Telescope). *Left*: Thin threads of an active region prominence in Ca II H line (λ3968 Å) bandpass observed with Hinode/SOT 2007 February 8 (*Credit*: Okamoto et al. 2007)

2.4.2   Quiescent Type Prominences

A commonly existing *quiescent prominence* is the hedgerow type consisting of long and tall blade-like palisades along the filament channels. The dimensions of a well-developed *quiescent prominence* are typically less than 5,000 km wide, 30,000 km high by 200,000 km long but both longer and shorter examples are readily found. Quiescent prominences are commonly located in high latitude regions ($\geq 50°$) in the polar crown filament channels which vary slightly in latitude and orientation throughout the solar sphere and over the solar cycle. The dominating structures of quiescent filaments are barbs with largely vertical threads. Some curtains of barb threads often end on arcs at the prominence base (cf. Martin et al. 2009), as shown in the left image of Fig. 2.10, which possibly also are related to so-called "*bright rims*" (Paletou 1997). The horizontally oriented spines in the higher regions of prominence body are generally rather faint in Hα but they appear a lot more pronounced in the hotter He II λ304 Å line (Wang et al. 1998; Lin 2000; Xu et al. 2010).

The persistent quiescent filaments occurring at high latitudes are commonly referred to as polar crown prominences. D'Azambuja and D'Azambuja (1948) concluded from comprehensive and careful investigations that quiescent prominences in their global appearance are exceedingly stable structures appearing at high latitudes and may last from weeks to several months. However, the continuous recent He II 304 Å observations from SOHO and SDO show that eruptions of segments of polar crown filaments are much more common than indicated from earlier and less frequent observations from ground-based observatories and quiescent prominences can develop at low latitudes as well as high latitudes. At low latitudes they are more likely to be destabilized as a result of being within 30 heliographic degrees of the site of a new active region (Feynman and Martin 1995).
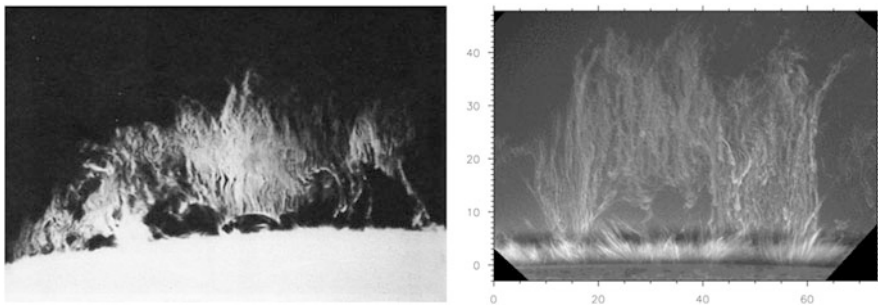

Fig. 2.10   *Left*: Quiescent prominences observed in Hα at the Sacramento Peak Observatory 1970 December 7 (*Credit*: NSO/NOAO). *Right*: Tall prominence observed in the Ca II H line λ3968 Å with Hinode/SOT 2007 October 3. The picture is scaled in arcseconds (*Credit*: Hinode/SOT)

2.4.3 Intermediate (Combined) Type Prominences

Intermediate filaments form between weak unipolar background fields regions and active regions or active region complexes and constitute a class in-between the other two. They also occur between and within decaying active regions. They have lengths of ∼100,000 km along the extended filament channels and do not necessarily occupy the full length of a channel. One part of an intermediate filament may have the appearance of the quiescent type while another part may have the resemblance of an AR filament. The upper right image of Fig. 2.8 shows part of a long *Intermediate* type filament located at N22E18 and at some distance from an active region on 27 August 2003. This filament has the characteristic continuous, slender body of the AR type and well developed fine-structured barbs typical for quiescent filaments. From many such examples, representative of I/EBR class of Mackay et al. (2008), it is clear that the differences in AR, intermediate and quiescent filaments are ones of scale or degree of activity rather than fundamental difference in their nature and physics.

2.4.4 Substructures

2.4.4.1 Threads

The characteristic fine structures of solar prominences were clearly noticeable in the fine drawings by the early solar observers (cf. Vial 2014), but these became more fully appreciated after the famous high resolution observations of Dunn (1960) displayed in time-lapsed movies. Similar type of prominence movies were earlier made by Robert McMath at the McMath–Hulbert Solar observatory. Recent high spatial and temporal resolution observations from ground-based observatories and telescopes in space have confirmed that the entire bodies of solar prominences consist of complex, rapidly changing fine structures. Spines consist of bundles of largely horizontally oriented threads and blobs subjected to *counterstreaming* motions (Zirker et al. 1998; Lin et al. 2003; Ahn et al. 2010; Berger 2013). The same fine threads and blobs continue into the barbs, which diverge from the spine at intervals resembling the photospheric supergranular cell sizes, and bend down into the photosphere below. High-resolution data shows that the structural sizes, e.g. thickness, of the small-scale structures vary from truly several arc sec down to the resolution limit of the best instruments, e.g. ≥0.15 arc sec (∼100 km), which implies that some structures may even be thinner.

The top view of two adjacent multi-thread filament barbs are displayed in Fig. 2.11. The Doppler image on the right demonstrates the presence of *counterstreaming*, both down- and up-flows in separate but adjacent, interleaved threads of plasma. The darkest regions in the intensity image correspond to the transition where the sharp and clear spine threads are curving steeply downward into the barbs
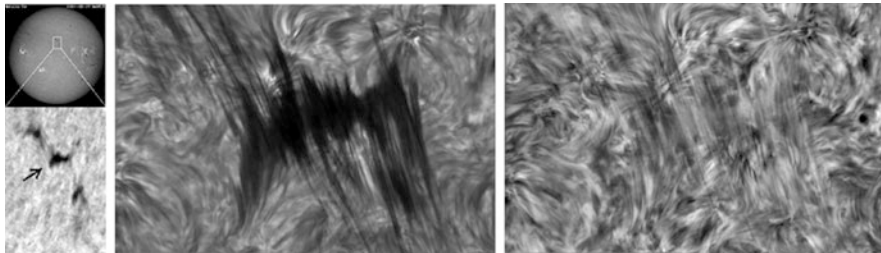
Fig. 2.11 The *middle panel* shows a high resolution Hα image of a barb of a fragmented hedgerow filament observed with the SST on August 22, 2004. The *arrow* in the *lower left image*, which was recorded with LESIA, Observatoire de Paris, indicates which one is the observed fragment. The high resolution image reveals a dark multi-thread, multi-footpoint barb on the *left* with sparse spine threads extending out of the image to the north while the dark barb threads on the *right* are associated with thin spine threads extending out of the image to the south. A few spine threads in the *middle* could be superposed against the dark barbs rather than being connected to them. The image to the right shows the corresponding Doppler image which is derived by subtracting the *red wing image* ($\Delta\lambda = +0.3$ Å) from the *blue wing* ($\Delta\lambda = -0.3$ Å) that make *blue-shifted* elements appear *bright* and *red-shifted dark* (*Credit*: Lin et al. 2007)

or vice-versa, the transition of the steep barb threads coming out in our line-of-sight into the horizontal spine. Therefore, the column density of the barb threads in the line-of-sight is higher than in the horizontal threads of the spine. At the left and right sides of the adjacent dextral barbs, one can see some locations where the barb threads connect to the chromosphere. However, in the bottom part of the barbs, many of the fine threads are too densely packed to be resolved even in these high quality SST images.

Berger (2013) points out that the threads appear somewhat thicker and more structured in prominences at the limb compared with the smooth threads seen against the disk (Lin et al. 2005a). Such differences between the on-disk filament threads and threads in off-limb prominences pose a challenge in interpretation and modeling of prominences. A possible solution to this problem could be that on-disk absorption in Hα is largely dependent on the population of the n = 2 energy level in the hydrogen atoms while the off-limb emission structures depend more on the n = 3 level population. The latter population is much more sensitive to variations in the thermodynamic parameters of the cool prominence plasma.

Besides the apparent internal flowing of plasma along the threads one observes sideways (swaying) motions of individual threads. Individual threads in barbs move sideways with speed 2–3 km s^{-1} (Lin et al. 2005a) which also compares well with the observed small-scale flow velocities of magnetic flux elements in the photosphere. Line-of-sight (LOS) Doppler motions at speeds of 5–10 km s^{-1} of individual prominence substructures were studied by Zirker and Koutchmy (1991).

The highly inclined oriented fine structure in barbs remains a key mystery in studies of prominence barbs. The appearance of smooth and elongated fine

structures in combination with flow velocities up to 15 km s^{-1} and higher would suggest that the flows are field-aligned and the orientation of the threads reflects the orientation of the magnetic fields, which includes the highly inclined ones as well. One does not observe free fall speeds of cool prominence plasma in highly inclined barbs. The vertical extent of barbs is much longer than the gravitational scale height of prominence plasma (∼200 km) which implies that the plasma must somehow be supported against gravity (Mackay et al. 2010). Steele and Priest (1992) and Aulanier and Démoulin (1998) modeled the thread structures as a series of sharply dipped magnetic field lines under magnetostatic conditions. However, static magnetic topologies seem incompatible with the morphological character of the thin threads as well as the observed flowing and counterstreaming of the plasma.

The ubiquitous presence of oscillations in solar prominences, off-limb as well as on-disk, led Pécseli and Engvold (2000) to study the possibility that damping of MHD waves might serve to accelerate the partly ionized cool plasma and thereby counteract and/or balance gravity. The presence of a necessary high frequency waves for this mechanism to work is still beyond the current limit of detection in solar observations.

2.4.4.2 Filling Factor

As discussed and shown above and elsewhere in this chapter (Figs. 2.9, 2.10 and 2.11) solar prominences are made up of numerous thin threads and small-scale droplets. The angular widths of the thinnest threads and other small-scale structures are comparable to the resolution limit of the best instruments today, i.e. ∼0.15 arcsec, which suggests that some threads may be even thinner. Thermodynamic modeling based on observed emission of prominences depends on the proper knowledge of the true volumes of the radiating plasma. Zirker and Koutchmy (1990) assumed a clustering of moving, unresolved, uniform, threads that reproduced the observed structures and concluded that the observed fine structures might consist of up to 20 single thinner threads along the line-of-sight. It is generally believed that the thinnest volumes of the cool plasma have thread-like shapes whereas the presumed thin *Prominence Corona Transition Region* (PCTR) must inevitably be more tube-like.

The effective radiating volume is referred to as the *filling factor* which thereby becomes a central parameter in interpretation and modeling of observed line emission from both the cool core and the PCTR of prominences. Mariska et al. (1979) and Widing et al. (1986) derived volume filling factors in the range 0.018–0.024. Cirigliano et al. (2004) concluded from observations of the PCTR with the SUMER instrument on SOHO that the *filling factor* may be as low as 10^{-3}.

The filling factor has remained an issue of concern in prominence modeling, which is discussed by Parenti (2014b) and Labrosse (2014).

2.4.4.3 Minifilaments

In the era of moderate spatial resolution (∼1 arcsec) and temporal resolution
(∼1 min) observers took note of a small-scale analogue to large-scale filaments
which are referred to as miniature filaments or commonly shortened to *minifilaments*
(Hermans and Martin 1986). From a detailed study of time-lapse datasets in Hα
obtained at Big Bear Solar Observatory Wang et al. (2000) concluded that a
typical *minifilament* of projected length around 20,000 km has a lifetime of 50 min
from first appearance through disappearance and eruption. Similar to large-scale
filaments, also *minifilaments* reside above local PILs. *Minifilaments* have a variety
of characteristics in common with AR filaments and quiescent filaments and may
serve as a proxy in studies of more complex systems (Denker and Tritschler 2009).

2.4.4.4 Pillars and "Tornadoes"

Tornado-like prominences resembling terrestrial tornadoes in shape when seen on
the solar limb were noticed by several observers (cf. Panasenco et al. 2014). Pettit
(1932) described these structures as "Vertical spirals or tightly twisted ropes" and
introduced tornado-like prominences as a separate class.

A group of tornado-like prominences structures at the solar limb shown in the left
panel of Fig. 2.12 were observed by the space instrument TRACE (cf. Vial 2014)
1999 November 27 (Panasenco et al. 2014). These pillar-looking structures which
appear to fan out in the tree-shaped structures are typical for barbs of large quiescent
prominences (Pevtsov and Neidig 2005; Lin et al. 2008) that are also classed as
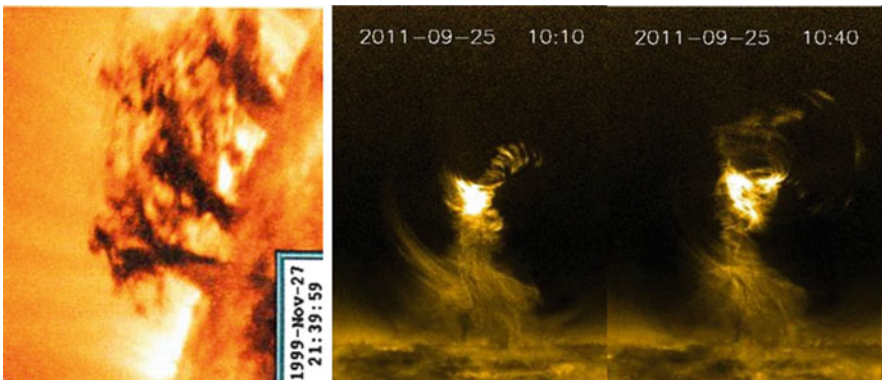hedgerow prominences by Menzel and Evans (1953).

Fig. 2.12 *Left image*: A group of tornado-like prominences observed by TRACE in the λ171 Å
line 1999 November 27 (*Credit*: Panasenco et al. 2014). The *right images* of a huge tornado-like
feature were captured by the Solar Dynamic Observatory which show a spectacular formation of a
dynamic event in the coronal cavity above a solar prominence (*Credit*: NASA/Li et al. 2012)

The development of a large tornado-like event was recorded with the SDO/AIA during 2011 September 24 through 26 (Li et al. 2012). Two examples of this feature recorded in the 171 Å line channel are also displayed in Fig. 2.12. The fascinating, long time coverage of this event showed its formation as a result of upward material flow from below which penetrated into the cavity above the prominence. The same event was studied by Panesar et al. (2013) who found that flare activity in a neighboring active region had an apparent causal relationship with this tornado-like event.

Su et al. (2012) and Wedemeyer-Böhm et al. (2012) concluded that tornado-like barbs are rooted in vortexes located at intersections of supergranulation cells where rotating magnetic structures could develop. In the following study Wedemeyer et al. (2013) concluded from combined 171 Å data of SDO/AIA and Hα observations with the SST that the legs (barbs) of prominences in pre-eruption phase appear associated with rotating tornados. The sideways oscillating appearance in 2-D of a such event does not necessarily prove the presence of spiraling motion which should be expected in the case of plasma motion in a tornado-like helical magnetic structure. Further clarification of this issue is foreseen. Panasenco et al. (2014) find that the apparent tornado-like structure and motion in hedgerow quiescent prominences may be fully explained as a combination of counterstreaming and oscillation.

Tornado-like features discussed by Li et al. (2012) and Panesar et al. (2013), and some of the tornados described by Pettit (1932), are transient and rapidly changing in overall structure compared with the apparently more stable pillars recorded with TRACE and presented above in Fig. 2.12 (Panasenco et al. 2014). Such differences in character, degree of activity and associated events may be indicators of different physical processes among the variety of features that have been called tornado prominences and point to the need for Doppler images from spectral data for more definitive interpretations.

2.4.5   Dynamics

2.4.5.1   Flows

High-resolution time series reveal ubiquitous flowing of the cool plasma along the thread directions. Zirker et al. (1998) detected a steady bidirectional streaming with typical speeds of 10–20 km s^{-1} everywhere along closely spaced threads in a large filament. The pattern was observed in both wings of Hα which confirmed that the flows are mass motions and not caused by some kind of excitation wave. This flow pattern, which is being referred to as *counterstreaming*, was confirmed in a later study by Lin et al. (2003). The same flow pattern is seen both in *spines* and in *barbs*. Engvold et al. (1985) detected systematic flows in the PCTR. Time series of Ca II H images from the filter pass band of Hinode/SOT confirm the presence of flows along spines and up and down in barbs (Ahn et al. 2010). Recent studies by

Alexander et al. (2013) using simultaneous observations of an active region filament in the λ193 Å line with the ultra-high spatial resolution (0.2 arcsec) and temporal resolution of the Hi–C (Cirtain et al. 2013) and the SDO/AIA instrument (He II λ304 Å and continuum λ ∼ 1,600 Å) find anti-parallel flows in threads (∼0.8 arcsec thick) at velocities as high as 70–80 km s^{-1}, which is notably higher than reported for the cool prominence plasma (see Fig. 4.6 in Kucera 2014).

It is generally accepted that mass flows at the speeds quoted above in assumed low-β plasma must inevitably be field-aligned and that the flow pattern thereby reflects the structure and orientation of the local magnetic fields.

A consequence of continuous streaming of the plasma through the entire prominence body is that in order to maintaining the mass through the observed lifetimes implies an approximate global balance between loss and inflow of plasma. Assuming typical lengths of quiescent prominences between 30,000 and 100,000 km and flow speed of ∼10 km s^{-1}, the entire mass of a prominence will be exchanged in the course of 1–3 h. Understanding the apparent ever-present flowing and its consequences remains a central issue in prominence studies.

Haerendel and Berger (2011) observed isolated knots or droplets of plasma from quiescent prominences to fall at near free fall speed at about 100 km s^{-1}. Similar features were studied and discussed by Hillier et al. (2012). Also most erupting prominences have similar rapidly streaming down flows of mass concurrent with the outward bodily transport of all or part of the prominence.

2.4.5.2 Oscillations

The oscillating nature of solar filaments was first noticed as bodily "winking filaments" with velocity amplitudes of 20 km s^{-1} and higher, shaken by flare generated waves (Ramsey and Smith 1966). Information on smaller-amplitude oscillations is usually derived from Doppler velocity data, in addition to high-resolution time series which also permit measurements of transverse (side-ways) swaying motion of filament threads (Lin et al. 2009). High resolution time series all show an ever-present oscillatory pattern in solar filaments.

Studies of small-amplitude periodic variations in line-of-sight motions in prominences, with the aim to understand the magnetic structures and interaction with the plasma, revealed the presence of a wide range of oscillatory periods (Molowny-Horas et al. 1999; Banerjee et al. 2007; Engvold 2008). Periods (P) < 10 min are referred to as short, while intermediate and long periods are, respectively, 10 min < P < 40 min and P > 40 min. Small-amplitude oscillations, $\Delta v = 0.1$–3 km s^{-1}, are detected at all periods, whereas large-amplitudes (20–40 km s^{-1}) are commonly observed at long periods. Small-amplitude oscillations are generally associated with individual threads, but they appear in addition to partly involve the entire filament body (Lin et al. 2003).

Lin et al. (2003) found evidence for traveling waves in the thread structure to move in the same direction as the mass flows. The presence of continuously generated, propagating groups of waves perpendicular to prominence magnetic
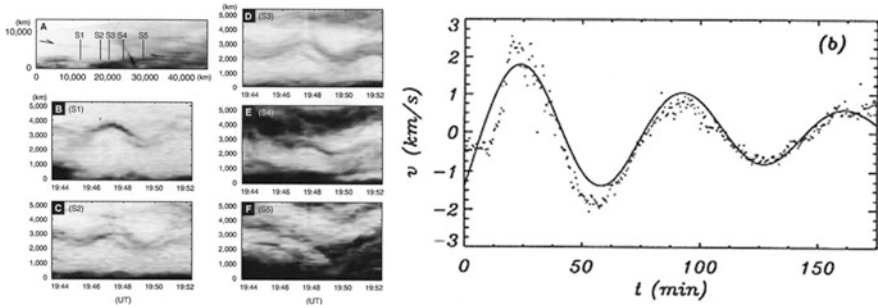
Fig. 2.13 *Left panel*: Examples of prominence threads undergoing synchronous oscillations along the spine of an AR prominence observed with Hinode/SOT 2007 February 8. Lines S1 to S5 indicate the locations of height versus time plots in the panels B to F (*Credit*: Okamoto et al. 2007). Right diagram: Damped long period oscillation in a quiescent prominence derived from Doppler velocity (*dots*) and fitted function (*continuous line*) versus time. The period is 70 min and the damping time is 101 min (*Credit*: Molowny-Horas et al. 1999)

field is confirmed also in a study by Schmieder et al. (2013). From Ca II H line ($\lambda 3968$ Å) band pass movies of an active region prominence (Fig. 2.13) Okamoto et al. (2004) examined six threads and detected vertical oscillatory motions with amplitudes in the plane of the sky ranging from 400 to 1,800 km. The horizontally oriented threads appeared to contain continuous horizontal flows at speeds in the range 15–46 km s^{-1}. These authors propose that the observed oscillations might represent propagating Alfvén waves along the horizontally oriented magnetic fields of this prominence. Chen et al. (2009) found evidence from EUV data that up-flows connected with *counterstreaming* are associated with stronger magnetic fluxes, e.g. brighter *plage* areas, while down-flows seem connected to a weaker flux.

The oscillatory amplitudes in solar filaments and prominences decrease with time and die out in the course of a few periods (right panel Fig. 2.14). This phenomenon is referred to as wave damping. The damping times range usually from one to three times the corresponding period (Oliver and Ballester 2002). The loss in wave energy indicated by wave damping in filaments might possibly be involved in accelerating the ever-present flowing of the partly ionized plasma. Alternative damping mechanisms are discussed in the review by Soler et al. (2014).

The main aim of prominence seismology is to infer and understand the internal structure and physical properties of solar prominences. Further details are given in reviews by Ballester (2006, 2014) and Lin (2011).

2.4.5.3 Prominence Plumes

Visible-light spectral observations of quiescent prominences exhibit plume-like features rising through them from the chromosphere/photosphere with the shape of "mushroom caps" at velocities in the range 20–30 km s^{-1}. They may start as a single
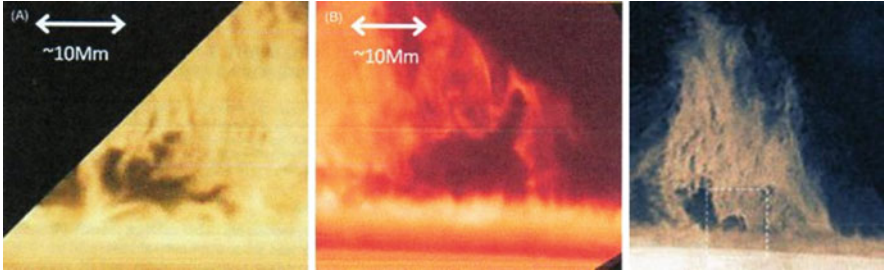
Fig. 2.14 *Left image*: Observations in Ca II H line of dark up-flows in a quiescent prominence on 2007 August 8. Middle image: A similar feature observed in Hα 2010 June 22. (*Credit*: Hiller et al. 2012). *Right image*: Quiescent prominence observed in 2007 in Hα at Mauna Loa Solar Observatory 2007 April 25, at 90W 36S heliographic coordinates. The white dashed box highlights an area of up-flow development in the prominence (*Credit*: T. Berger et al. 2010)

∼10,000 km large plume, or bubble, which occasionally breaks up into smaller ones. In SDO/AIA λ193 Å images the plumes appear slightly brighter than in the prominence itself but notably less bright than the corona outside the prominences (Dudik et al. 2012).

Plumes in quiescent prominences were first reported by Stellmacher and Wiehr (1973) and later studied in detail by Berger et al. (2008, 2010, 2011) in observations from the Hinode satellite. It is generally thought that prominence plumes represent under-dense plasma relative to the ordinary prominence plasma and give rise to Rayleigh–Taylor buoyancy instability (Ryutova et al. 2010). The assumed magneto-convective (plasma-$\beta \approx 1$) plume features have been observed to rise into the overlying coronal cavities but their influence on cavity evolution is yet unclear (Berger et al. 2011).

Plumes are not yet identified in *Intermediate* and *AR* type prominences (Berger 2013).

2.4.5.4 The Eruptive Phase of Solar Prominences

The early phase of prominence eruptions is noticed as a *slow rise* at speeds of about 0.1–1 km s^{-1} several hours before its actual eruption (Sterling and Moore 2004; Isobe et al. 2007), after which it undergoes rapid upward acceleration to velocities ranging from 100 to 1,000 km s^{-1}. Erupting prominences leave behind concurrently formed flare loops and post-flare loops that straddle the vacated filament channel. They are accompanied by the expulsion of overlying and surrounding coronal loop systems that develop into *Coronal Mass Ejections* (*CMEs*). In the final stage the CME structure expands at nearly constant speed (Liu et al. 2009). The leading front continues its fast outward motion while fractions of the core material are occasionally seen to collapse back towards the Sun (Wang and Sheeley 2002). In two

thirds of observed cases prominences reform in the same prominence or filament channel, with a similar shape in the course of 1–7 days.

Occasionally, and very likely depending on the magnetic environment, only parts of a prominences erupt as one part stays anchored in the channel while the rest undergoes eruption (Liu et al. 2009). In other eruptive events only the higher filament body may take part in the pre-eruptive *slow rise* and subsequent eruption (Liu et al. 2012c).

A number of structural and dynamic changes, in addition to the slow rise, signal the beginning of an erupting event. Some polar crown filaments exhibit large amplitude oscillations during the pre-eruption slow-rise phase (Isobe and Tripathi 2006). Spectral changes are often observed both in emission and absorption in the early phase of an eruption. Both active region and quiescent prominences exhibit enhanced non-thermal motions and become darker (when viewed on the disk as filaments) and brighter (when viewed at the limb). Observations of highly ionized EUV lines show increased emission in conjunction with prominence eruption (Engvold et al. 2001) (Fig. 2.15).

Much attention has been given to understanding the triggering of eruptive prominences (van Driel-Gesztelyi and Culhane 2009; Parenti 2014a). Some of the common mechanisms proposed as triggers for solar events are interactions with emerging magnetic flux (Bruzek 1952; Feynman and Martin 1995; Wang and Sheeley 1999), interactions of prominence fields with overlying coronal fields (Antiochos et al. 1999), interactions of the root fields of prominences with adjacent magnetic fields (Nagashima et al. 2007), and in relatively rare cases, being hit by flare waves (Okamoto et al. 2004; Isobe et al. 2007) and long-term effects associated with observed cancelling magnetic fields (Martin et al. 1985, 2012). The review by Aulanier (2014) provides a detailed evaluation of various proposed mechanisms for prominence eruptions.
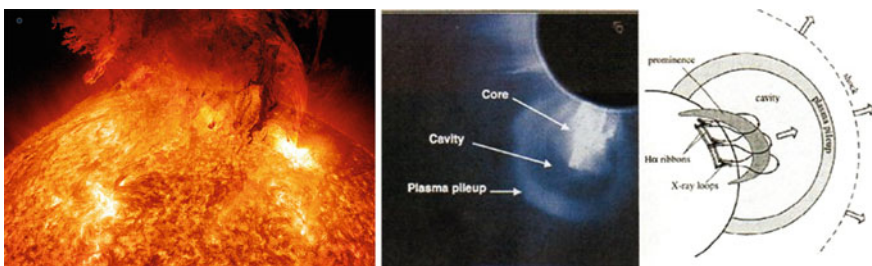

Fig. 2.15 *Left image*: A huge prominence eruption observed with SDO on June 7, 2011 (*Credit*: NASA/SDO/J. Major). *Middle image*: A Solar Maximum Mission archive image showing the principal features of an erupting prominence and a CME (Hundhausen 1999). *Right panel*: Schematic view of a CME (Credit: Forbes 2000)
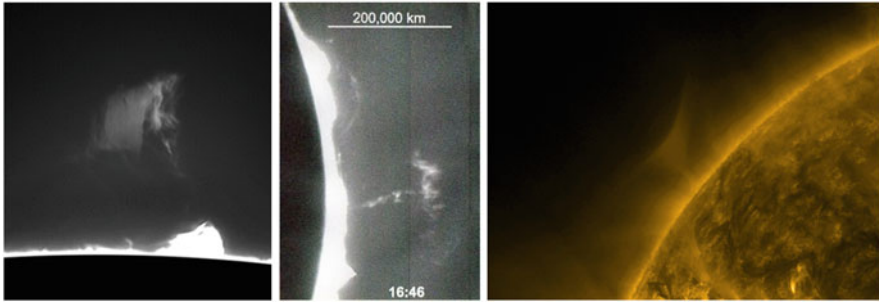
Fig. 2.16 Hα images Coronal Cloud Prominences; the *left image* of 26 August 2013 (*Credit*: James Ferreira) and the *middle image* was obtained at Helio Research on September 17, 2004 (*Credit*: Helio Research). The *right image* shows a funnel prominences of 28 April 2012 obtained in 171Å with SDO/AIA (*Credit*: NASA/SDO)

2.5 Coronal Cloud Prominences and Coronal Rain

Coronal cloud prominences are cool material suspended up to 200,000 km in the corona. This is rather high in comparison to stable quiescent prominences which rarely exceed 35–50,000 km during their non-erupting state. Allen et al. (1998) studied the structure and kinematics of a number of such prominences and referred to them as "*coronal spiders*" due to their characteristic shape. Coronal cloud prominences have also been termed "*funnel prominences*" because of a characteristic V-shaped structure (Liu et al. 2012b) which might be due to one particular view angle of an asymmetric structure. In some cases the V-shape is preceded by or followed by an expansion of the cloud feature into a spider-like shape.

Coronal cloud prominences do not erupt. On the contrary, they shrink and disappear within a few hours to a day from drainage along well-defined curved trajectories at close to free-fall speeds resembling coronal rain. This prominence type has only been seen above the limb to date and they are evidently too weakly absorbing to be observable against the disk. Otherwise, they might be considered common instead of relatively uncommon (see Martin 2014).

Available observations suggest that cloud prominences become visible in 304 Å or Hα resulting from radiative cooling instabilities (Karpen and Antiochos 2008) in magnetized coronal plasma when thermal conduction becomes effectively inhibited by local changes in magnetic field configuration. The formation process is not yet fully understood and is a subject for further investigation (Fig. 2.16).

The physical nature of Coronal Cloud Prominences appears to differ in several respects from more common, regular channel associated type prominences. Also, there is so far no evidence for them to be associated with PILs.

"*Coronal rain*" is observed to come from coronal cloud prominences and in addition seen to condense directly out of the thin, hot corona. This phenomenon was first observed in Hα as cascades of small, bright packets of matter streaming

down along trajectories that closely outline the orientation of the pervasive magnetic fields. From recent observations of fine structured loops Antolin and Rouppe van der Voort (2012) conclude that *coronal rain* is a common phenomenon seen in the low temperature lines Hα and Ca II H, with an average falling speed around 70 km s^{-1} and an acceleration notably below free fall. Schrijver (2001) followed the various shapes of coronal rain formation at speed up to 100 km s^{-1} in coronal loops from pass bands of the TRACE instruments, from a few million degrees down to less than 100,000 K. Coronal rain appears closely associated to solar flares which suggest that the triggering mechanisms of these two phenomena are connected. The two seemingly different sources of coronal rain may result from variations in magnetic topology in the coronal regions at stake, which either may support the formation of a coronal cloud prominence that subsequently are drained via the rain, or the condensing matter is drained as quickly as the apparent condensation takes place.

References

Ahn, K., Chae, J., Cao, W., & Goode, P. R. (2010). Patterns of flows in an intermediate prominence observed by Hinode. *The Astrophysical Journal, 721*, 74–79.

Alexander, C. E., Walsh, R. W., Régnier, S., Cirtain, J., et al. (2013). Anti-parallel EUV flows observed along active region filament threads with Hi-C. *The Astrophysical Journal, 775*, L32–L38.

Allen, U. A., Bagenal, F., & Hundhausen, A. J. (1998). Analysis of Hα observations of high altitude coronal condensations, new perspectives on solar prominences. In D. F. Webb, B. Schmieder, & D. M. Rust (Eds.), *ASP conference series, IAU colloquium 167* (Vol. 150, p. 290).

Antiochos, S. K., DeVore, C. R., & Klimchuk, J. A. (1999). A model for solar coronal mass ejections. *The Astrophysical Journal, 510*, 485–493.

Antolin, P., & Rouppe van der Voort, L. (2012). Observing the fine structure of loops through high-resolution spectroscopic observations of coronal rain with the CRISP instrument at the Swedish solar telescope. *The Astrophysical Journal, 745*, 152–173.

Anzer, U., Heinzel, P., & Fárnik, F. (2007). Prominences on the limb: Diagnostics with UV EUV lines and the soft X-ray continuum. *Solar Physics, 242*, 43–52.

Aulanier, G. (2014). The physical mechanisms that initiate and drive solar eruptions. In *IAU symposium* (Vol. 300, pp. 184–196).

Aulanier, G., & Demoulin, P. (1998). 3-D magnetic configurations supporting prominences. I. The natural presence of lateral feet. *Astronomy and Astrophysics, 329*, 1125–1137.

Ballester, J. L. (2006). Seismology of prominence-fine structures: Observations and theory. *Space Science Reviews, 122*, 129–135.

Ballester, J. L. (2014). Magnetism and solar prominences: MHD waves. In J.-C. Vial, & O. Engvold (Eds.), *Solar Prominences, ASSL* (Vol. 415, pp. 257–294). Springer.

Banerjee, D., Erdélyi, R., Oliver, R., & O'Shea, E. (2007). Present and future observing trends in atmospheric magnetoseismology. *Solar Physics, 246*, 3–29.

Berger, T. (2013). Solar prominence fine structure and dynamics. Nature of prominences and their role in space weather. In *Proceedings of the IAU symposium* (Vol. 300, pp. 15–29).

Berger, T. E., Shine, R. A., Slater, G. L., et al. (2008). Hinode SOT observations of solar quiescent prominence dynamics. *The Astrophysical Journal, 676*, L89–L92.

Berger, T. E., Slater, G., Hurlburt, N., et al. (2010). Quiescent prominence dynamics observed with the Hinode solar optical telescope. I. Turbulent upflow plumes. *The Astrophysical Journal, 716*, 1288–1307.

Berger, T., Testa, P., Hillier, A., et al. (2011). Magneto-thermal convection in solar prominences. *Nature, 472*, 197–200.

Berger, T. E., Liu, W., & Low, B. C. (2012). SDO/AIA detection of solar prominence formation within a coronal cavity. *The Astrophysical Journal, 758*, L37.

Bommier, V., Landi Degl'Innocenti, E., Leroy, J.-L., & Sahal-Brechot, S. (1994). Complete determination of the magnetic field vector and of the electron density in 14 prominences from linear polarization measurements in the HeI D3 and Hα lines. *Solar Physics, 154*, 231–260.

Bruzek, A. (1952). Die Ausbreitung von "Euptionsstörungen". Mit 2 Textabbildungen. *Zeitschrift für Astrophysik, 31*, 111.

Chae, J., Wang, H., Qiu, J., Goode, P. R., Strous, L., & Yun, H. S. (2001). The formation of a prominence in active region NOAA 8668. I. SOHO/MDI observations of magnetic field evolution. *The Astrophysical Journal, 560*, 476–489.

Chen, H., Jiang, Y., & Ma, S. (2009). An EUV jet and Hα filament eruption associated with flux cancelation in a decaying active region. *Solar Physics, 255*, 79–90.

Cirigliano, D., Vial, J.-C., & Rovira, M. (2004). Prominence corona transition region plasma diagnostics from SOHO observations. *Solar Physics, 223*, 321–351.

Cirtain, J. W., Golub, L., Winebarger, A. R., et al. (2013). Energy release in the solar corona from spatially resolved magnetic braids. *Nature, 493*, 501–503.

D'Azambuja, L., & D'Azambuja, M. (1948). *A comprehensive study of solar prominences and their evolution from spectroheliograms obtained at the observatory and from synoptic maps of the chromosphere published at the institution* (Vol. 6, part 7). Ann. Obs. Paris-Meudon.

de Jager, C. (1959). Structure and dynamics of the solar atmosphere. *Handbuch der Physik, 52*, 80.

Denker, C., & Tritschler, A. (2009). Mini-filaments – small-scale analogues of solar eruptive events? In *IAU symposium* (Vol. 259, pp. 223–224).

Deslandres, H. (1910). *Recherches Sur l'Atmosphère Solaire; Photographies des Couches Gazeuses Supèriures* (IV(I), pp. 1–139) Ann. Obs. Paris-Meudon.

Dudík, J., Aulanier, G., Schmieder, B., Zapiór, M., & Heinzel, P. (2012). Magnetic topology of bubbles incbrr quiescent prominences. *The Astrophysical Journal, 761*, 9–22.

Dunn, R. (1960). *Photometry of the solar chromosphere*, Ph.D. Thesis, Harvard University.

Engvold, O. (2008). Observational aspects of prominence oscillations. In *IAU symposium* (Vol. 247, pp. 152–157).

Engvold, O., Tandberg-Hanssen, E., & Reichmann, E. (1985). Evidence for systematic flows in the transition region around prominences. *Solar Physics, 96*, 35–51.

Engvold, O., Jakobsson, H., Tandberg-Hanssen, E., Gurman, J. B., & Moses, D. (2001). On the nature of prominence absorption and emission in highly ionized iron and in neutral hydrogen. *Solar Physics, 202*, 293–308.

Feynman, J., & Martin, S. F. (1995). The initiation of coronal mass ejections by newly emerging magnetic flux. *Journal of Geophysical Research, 100*, 3355–3367.

Forbes, T. G. (2000). A review on the genesis of coronal mass ejections. *Journal of Geophysical Research, 105*, 23153–23166.

Foukal, P. (1971). Morphological relationships in the chromospheric Hα fine structure. *Solar Physics, 19*, 59–71.

Fuller, J., Gibson, S. E., de Toma, G., & Fan, Y. (2008). Observing the unobservable? Modeling coronal cavity densities. *The Astrophysical Journal, 678*, 515–530.

Gaizauskas, V. (1998). Filament channels: Essential ingredients for filament formation (review). In *ASP conference series* (Vol. 150, pp. 257–264).

Gibson, S. (2014). Coronal cavities: Observations and implications for the magnetic environment of prominences. In J.-C. Vial, & O. Engvold (Eds.), *Solar prominences*. Springer.

Gibson, S. E., Kucera, T. A., Rastawicki, D., et al. (2010). Three-dimensional morphology of a coronal prominence cavity. *The Astrophysical Journal, 724*, 1133–1146.

Habbal, S. R., Druckmüller, M., Morgan, H., et al. (2010). Total solar eclipse observations of hot prominence shrouds. *The Astrophysical Journal, 719*, 1362–1369.

Haerendel, G., & Berger, T. (2011). A droplet model of quiescent prominence downflows. *The Astrophysical Journal, 731*, 82.

Hale, G. E. (1903). The snow horizontal telescope. *The Astrophysical Journal, 17*, 314.

Hale, G. E. (1929). The spectrohelioscope and its work. *The Astrophysical Journal, 70*, 265.

Heinzel, P. (2014). Radiative transfer in solar prominences. In J.-C. Vial, & O. Engvold (Eds.)*, Solar prominences, ASSL* (Vol. 415, pp. 101–128). Springer.

Heinzel, P., Schmieder, B., Fárník, F., et al. (2008). Hinode, TRACE, SOHO, and ground-based observations of a quiescent prominence. *The Astrophysical Journal, 686*, 1383–1396.

Hermans, L. M., & Martin, S. F. (1986). Small-scale eruptive filaments on the quiet sun. *BAAS, 18*, 991.

Hillier, A., Isobe, H., Shibata, K., & Berger, T. (2012). Numerical simulations of the magnetic Rayleigh–Taylor instability in the Kippenhahn–Schlüter prominence model. II. Reconnection-triggered downflows. *The Astrophysical Journal, 756*, 110–120.

Hirayama, T. (1985). Modern observations of solar prominences. *Solar Physics, 100*, 415–434.

Hundhausen, A. (1999). Coronal mass ejections. In K. T. Strong, J. L. R. Saba, B. M. Haisch, & J. T. Schmelz (Eds.), *The many faces of the sun: A summary of the results from NASA's solar maximum mission* (p. 143). New York: Springer.

Isobe, H., & Tripathi, D. (2006). Large amplitude oscillation of a polar crown filament in the pre-eruption phase. *Astronomy and Astrophysics, 449*, L17–L20.

Isobe, H., Tripathi, D., Asai, A., & Jain, R. (2007). Large-amplitude oscillation of an erupting filament as seen in EUV, Hα, and microwave observations. *Solar Physics, 246*, 89–99.

Karpen, J. T., & Antiochos, S. K. (2008). Condensation formation by impulsive heating in prominences. *The Astrophysical Journal, 676*, 688.

Kucera, T. A. (2014). Derivations and observations of prominence bulk motions and mass. In J.-C. Vial, & O. Engvold (Eds.)*, Solar prominences, ASSL* (Vol. 415, pp. 77–99). Springer.

Kucera, T. A., Gibson, S. E., Schmit, D. J., Landi, E., & Tripathi, D. (2012). Temperature and extreme-ultraviolet intensity in a coronal prominence cavity and streamer. *The Astrophysical Journal, 757*, 73.

Labrosse, N. (2014). Derivation of major properties of prominences using non-LTE modeling. In J.-C. Vial, & O. Engvold (Eds.)*, Solar prominences, ASSL* (Vol. 415, pp. 129–153). Springer.

Labrosse, N., Heinzel, P., Vial, J.-C., Kucera, T., Parenti, S., Gunár, S., Schmieder, B., & Kilper, G. (2010). Physics of solar prominences: I—Spectral diagnostics and non-LTE modelling. *Space Science Reviews, 151*, 243–332.

Leroy, J.-L. (1981). Simultaneous measurement of the polarization in Hα and D3 prominence emissions. *Solar Physics, 71*, 285–297.

Leroy, J. L. (1989). Observation of prominence magnetic fields. *Astrophysics and Space Science Library, 150*, 77.

Li, X., Morgan, H., Leonard, D., & Jeska, L. (2012). A solar tornado observed by AIA/SDO: Rotational flow and evolution of magnetic helicity in a prominence and cavity. *The Astrophysical Journal, 752*, L22–L27.

Lin, Y. (2000). *Comparison of Hα and He II 304 Å brightness variation in solar prominences*. MA Thesis, Institute of Theoretical Astrophysics, University of Oslo.

Lin, Y. (2011). Filament thread-like structures and their small-amplitude oscillations (invited review). *Space Science Reviews, 158*, 237.

Lin, Y., Engvold, O., & Wiik, J. E. (2003). Counterstreaming in a large polar crown filament. *Solar Physics, 216*, 109–120.

Lin, Y., Engvold, O., Rouppe van der Voort, L., Wiik, J. E., & Berger, T. E. (2005a). Thin threads of solar filaments. *Solar Physics, 226*, 431–451.

Lin, Y., Wiik, J. E., Engvold, O., Rouppe van der Voort, L., & Frank, Z. A. (2005b). Solar filaments and photospheric network. *Solar Physics, 227*, 283–297.

Lin, Y., Engvold, O., Rouppe van der Voort, L. H. M., & van Noort, M. (2007). Evidence of traveling waves in filament threads. *Solar Physics, 246*, 65–72.

Lin, Y., Martin, S. F., & Engvold, O. (2008). Filament substructures and their interrelation. In *ASP conference series* (Vol. 383, p. 235).

Lin, Y., Soler, R., Engvold, O., Ballester, J. L., Langangen, Ø., Oliver, R., & Rouppe van der Voort, L. H. M. (2009). Swaying threads of a solar filament. *The Astrophysical Journal, 704*, 870–876.

Liu, R., Alexander, D., & Gilbert, H. R. (2009). Asymmetric eruptive filaments. *The Astrophysical Journal, 691*, 1079–1091.

Liu, J., Zhou, Z., Wang, Y., Liu, R., et al. (2012a). Slow magnetoacoustic waves observed above a quiet-sun region in a dark cavity. *The Astrophysical Journal, 758*, L26–L32.

Liu, W., Berger, T. E., & Low, B. C. (2012b). First SDO/AIA observation of solar prominence formation following an eruption: Magnetic dips and sustained condensation and drainage. *The Astrophysical Journal, 745*, L21–L29.

Liu, R., Kliem, B., Török, T., et al. (2012c). Slow rise and partial eruption of a double-decker filament. I. Observations and interpretation. *The Astrophysical Journal, 756*, 59–73.

Lopez Ariste, A. (2014). Magnetometry of prominences. In J.-C. Vial, & O. Engvold (Eds.), *Solar prominences, ASSL* (Vol. 415, pp. 177–202). Springer.

Mackay, D. (2014). Formation of large-scale pattern of filament channels and filaments. In J.-C. Vial, & O. Engvold (Eds.), *Solar prominences, ASSL* (Vol. 415, pp. 353–378). Springer.

Mackay, D. H., Gaizauskas, V., & Yeates, A. R. (2008). Where do solar filaments form?: Consequences for theoretical models. *Solar Physics, 248*, 51–65.

Mackay, D. H., Karpen, J. T., Ballester, J. L., Schmieder, B., & Aulanier, G. (2010). Physics of solar prominences: II—Magnetic structure and dynamics. *Space Science Reviews, 151*, 333–399.

Mariska, J. T., Doschek, G. A., & Feldman, U. (1979). Extreme-ultraviolet limb spectra of a prominence observed from SKYLAB. *The Astrophysical Journal, 232*, 929–939.

Martin, S. F. (1998a). Conditions for the formation and maintenance of filaments (invited review). *Solar Physics, 182*, 107–137.

Martin, S. F. (1998b). Filament Chirality: A Link Between Fine-Scale and Global Patterns (Review). *ASP Conference Series, 150*, 419–429.

Martin, S. (2014). The magnetic field structure of prominences from direct and indirect observations. In J.-C. Vial, & O. Engvold (Eds.)*, Solar prominences, ASSL* (Vol. 415, pp. 203–233). Springer.

Martin, S. F., & Echols, C. R. (1994). An observational and conceptual model of the magnetic field of a filament. In R. J. Rutten & C. J. Schrijver (Eds.), *Solar surface magnetism [NATO Advanced Research Workshop]* (p. 339). Dordrecht: Kluwer Academic Publishers.

Martin, S. F., Livi, S. H. B., & Wang, J. (1985). The cancellation of magnetic flux. II – In a decaying active region. *Australian Journal of Physics, 38*, 929–959.

Martin, S. F., Marquette, W. H., & Bilimoria, R. (1992). The solar cycle pattern in the direction of the magnetic field along the long axes of polar filaments, the solar cycle. In *ASP conference series* (Vol. 27, p. 53).

Martin, S. F., Bilimoria, R., & Tracadas, P. W. (1994). Magnetic field configurations basic to filament channels and filaments. In R. J. Rutten & C. J. Schrijver (Eds.), *Solar surface magnetism* (p. 303). Dordrecht: Kluwer Academic Publishers.

Martin, S. F., Lin, Y., & Engvold, O. (2008). A method of resolving the 180-degree ambiguity by employing the chirality of solar features. *Solar Physics, 250*, 31–51.

Martin, S. F., Panasenco, O., Agah, Y., Engvold, O., & Lin, Y. (2009). Relating a prominence observed from the solar optical telescope on the Hinode satellite to known 3-D structures of filaments. In *ASP conference series* (Vol. 415, p. 183).

Martin, S. F., Panasenco, O., Berger, M. A., et al. (2012). The build-up to eruptive solar events viewed as the development of chiral systems. In *ASP conference proceedings* (Vol. 463, p. 157).

Menzel, D. H., & Evans, J. W. (1953). *Acad. Naz. Lincei. Conv. Volta*, *11*, 119.

Molowny-Horas, R., Wiehr, E., Balthasar, H., Oliver, R., & Ballester, J. L. (1999). *Prominence Doppler oscillations*. JOSO annual report, 1998, pp. 126–127.

Nagashima, K., Isobe, H., Yokoyama, T., Ishii, T. T., Okamoto, T. J., & Shibata, K. (2007). Triggering Mechanism for the Filament Eruption on 2005 September 13 in NOAA Active Region 10808. *The Astrophysical Journal, 668*, 533–545.

Newton, H. W. (1935). Note on two allied types of chromospheric eruption. *MNRAS, 95*, 650.

Okamoto, T. J., Nakai, H., Keiyama, A., Narukage, N., UeNo, S., Kitai, R., Kurokawa, H., & Shibata, K. (2004). Filament oscillations and Moreton waves associated with EIT waves. *The Astrophysical Journal, 608*, 1124–1132.

Okamoto, T. J., Tsuneta, S., Berger, T. E., et al. (2007). Coronal transverse magnetohydrodynamic waves in a solar prominence. *Science, 318*, 1577.

Okamoto, T. J., Tsuneta, S., & Berger, T. E. (2010). A rising cool column as a signature of helical flux emergence and formation of prominence and coronal cavity. *The Astrophysical Journal, 719*, 583–590.

Oliver, R., & Ballester, J. L. (2002). Oscillations in quiescent solar prominences observations and theory (invited review). *Solar Physics, 206*, 45–67.

Paletou, F. (1997). On Hα source function vertical variations in filaments and bright rims visibility. *Astronomy and Astrophysics, 317*, 244–247.

Panasenco, O., Martin, S. F., & Velli, M. (2014). Apparent solar tornado-like prominences. *Solar Physics, 289*, 603–622.

Panesar, N. K., Innes, D. E., Tiwari, S. K., & Low, B. C. (2013). A solar tornado triggered by flares? *Astronomy and Astrophysics, 549*, 105–110.

Parenti, S. (2014a). Solar prominences: Observations. Living Reviews in *Solar Physics, 11*, 1–88.

Parenti, S. (2014b). Spectral diagnostics of cool and PCTR optically thin plasma. In J.-C. Vial, & O. Engvold (Eds.), *Solar prominences, ASSL* (Vol. 415, pp. 61–76). Springer.

Parenti, S., & Vial, J.-C. (2007). Prominence and quiet-sun plasma parameters derived from FUV spectral emission. *Astronomy and Astrophysics, 469*, 1109–1115.

Pécseli, H., & Engvold, O. (2000). Modeling of prominence threads in magnetic fields: Levitation by incompressible MHD waves. *Solar Physics, 194*, 73–86.

Pettit, E. (1932). Characteristic features of solar prominences. *The Astrophysical Journal, 76*, 9.

Pevtsov, A. A., & Neidig, D. (2005). Accumulation of filament material at the boundaries of supergranular cells. In K. Sankarasubramanian, M. Penn, & A. Pevtsov (Eds.), *ASP conference series* (Vol. 346, p. 219).

Plocieniak, S., & Rompolt, B. (1973). Positions of filament feet in relation to the supergranular calcium network. *Solar Physics, 29*, 399–401.

Poland, A. I., & Tandberg-Hanssen, E. (1983). Physical conditions in a quiescent prominence derived from UV spectra obtained with the UVSP instrument on the SMM. *Solar Physics, 84*, 63–70.

Ramsey, H. E., & Smith, S. F. (1966). Flare-initiated filament oscillations. *Astronomical Journal, 71*, 197.

Ryutova, M., Berger, T., Frank, Z., Tarbell, T., & Title, A. (2010). Observation of plasma instabilities in quiescent prominences. *Solar Physics, 267*, 75–94.

Schmieder, B., Kucera, T. A., Knizhnik, K., Luna, M., Lopez-Ariste, A., & Toot, D. (2013). Propagating waves transverse to the magnetic field in a solar prominence. *The Astrophysical Journal, 777*, 108–119.

Schmit, D. J., Gibson, S. E., Tomczyk, S., Reeves, K. K., Sterling, A. C., Brooks, D. H., Williams, D. R., & Tripathi, D. (2009). Large-scale flows in prominence cavities. *The Astrophysical Journal, 700*, L96–L98.

Schrijver, C. J. (2001). Catastrophic cooling and high-speed downflow in quiescent solar coronal loops observed with TRACE. *Solar Physics, 198*, 325–345.

Sheeley, N. R., Jr., & Warren, H. P. (2012). Coronal cells. *The Astrophysical Journal, 749*, 40–54.

Sheeley, N. R., Jr., Martin, S. F., Panasenco, O. & Warren, H. P. (2013). Using coronal cells to infer the magnetic field structure and chirality of filament channels. *Astrophysical Journal, 772*, 88–99.

Simon, G. W., & Leighton, R. B. (1964). Velocity fields in the solar atmosphere. III. Large-scale motions, the chromospheric network, and magnetic fields. *The Astrophysical Journal, 140*, 120.

Smith, S. F. (1968). The formation, structure and changes in filaments in active regions. In *IAU symposium* (Vol. 35, p. 267).

Soler, R., Oliver, R., & Ballester, J. L. (2014). The damping of transverse oscillations of prominence threads: A comparative study. In *IAU symposium* (Vol. 300, pp. 48–51).

Steele, C. D. C., & Priest, E. R. (1992). A model for the fibril structure of normal-polarity solar prominences. *Solar Physics, 140*, 289–306.

Stellmacher, G., & Wiehr, E. (1973). Observation of an instability in a "Quiescent" prominence. *Astronomy and Astrophysics, 24*, 321.

Sterling, A. C., & Moore, R. L. (2004). Evidence for gradual external reconnection before explosive eruption of a solar filament. *The Astrophysical Journal, 602*, 1024–1036.

Su, Y., Wang, T., Veronig, A., Temmer, M., & Gan, W. (2012). Solar magnetized "Tornadoes:" Relation to filaments. *The Astrophysical Journal, 756*, L41–L48.

Tandberg-Hanssen, E. A. (1974). *Solar prominences*. Dordrecht: D. Reidel Publ. Co.

Tandberg-Hanssen, E. (1995). The nature of solar prominences. In *Astrophysics and Space Science Library* 199. Kluwer Academic Publishers.

Tang, F. (1987). Quiescent prominences – Where are they formed? *Solar Physics, 107*, 233–237.

van Driel-Gesztelyi, L., & Culhane, J. L. (2009). Magnetic flux emergence, activity, eruptions and magnetic clouds: Following magnetic field from the sun to the heliosphere. *Space Science Reviews, 144*, 351–381.

Vial, J. C. (1990). The prominence–corona interface. *Lecture Notes in Physics, 363*, 106–119.

Vial, J.-C. (2014). Historical background and introduction. In J.-C. Vial, & O. Engvold (Eds.), *Solar prominences, ASSL* (Vol. 415, pp. 1–29). Springer.

Waldmeier, M. (1970). The structure of the monochromatic corona in the surroundings of prominences. *Solar Physics, 15*, 167–175.

Wang, Y.-M., & Sheeley, N. R., Jr. (1999). Filament eruptions near emerging bipoles. *The Astrophysical Journal, 510*, L157–L160.

Wang, Y.-M., & Sheeley, N. R., Jr. (2002). Observations of core fallback during coronal mass ejections. *The Astrophysical Journal, 567*, 1211–1224.

Wang, H., Chae, J., Gurman, J. B., & Kucera, T. A. (1998). Comparison of prominences in Hα and He II 304 Å. *Solar Physics, 183*, 91–96.

Wang, J., Li, W., Denker, C., Lee, C., Wang, H., Goode, P. R., McAllister, A., & Martin, S. F. (2000). Minifilament eruption on the quiet sun. I. Observations at Hα central line. *The Astrophysical Journal, 530*, 1071–1084.

Wedemeyer, S., Scullion, E., Rouppe van der Voort, L., Bosnjak, A., & Antolin, P. (2013). Are giant tornadoes the legs of solar prominences? *The Astrophysical Journal, 774*, 123–138.

Wedemeyer-Böhm, S., Scullion, E., Steiner, O., et al. (2012). Magnetic tornadoes as energy channels into the solar corona. *Nature, 486*, 505–508.

Widing, K. G., Feldman, U., & Bhatia, A. K. (1986). The extreme-ultraviolet spectrum (300–630 A) of an erupting prominence observed from SKYLAB. *The Astrophysical Journal, 308*, 982–992.

Wood, P., & Martens, P. (2003). Measurements of flux cancellation during filament formation. *Solar Physics, 218*, 123–135.

Xu, Y., Jing, J., & Wang, H. (2010). Measurements of filament height in Hα and EUV 304 Å. *Solar Physics, 264*, 81–91.

Zirin, H. (1966). *The solar atmosphere*. Waltham, MA: Blaisdell-Ginn.

Zirin, H. (1988). *Astrophysics of the sun*. Cambridge: Cambridge University Press.

Zirin, H., & Tandberg-Hanssen, E. (1960). Physical conditions in limb flares and active prominences. IV. Comparison of active and quiescent prominences. *The Astrophysical Journal, 131*, 717.

Zirker, J. B., & Koutchmy, S. (1990). Prominence fine structure. *Solar Physics, 127*, 109–118.

Zirker, J. B., & Koutchmy, S. (1991). Prominence fine structure. II – Diagnostics. *Solar Physics, 131*, 107–118.

Zirker, J. B., Engvold, O., & Martin, S. F. (1998). Counter-streaming gas flows in solar prominences as evidence for vertical magnetic fields. *Nature, 396*, 440–441.